Explicit Gain Equations for Single Crystalline Photoconductors

Jiajing He,[§] Kaixiang Chen,[§] Chulin Huang, Xiaoming Wang, Yongning He, and Yaping Dan*

Read Online

ACCESS | 📊 Metrics & More | 📰 Article Recommendations | 🆘 Supporting Information

ABSTRACT: Photoconductors based on semiconducting thin films, nanowires, and two-dimensional atomic layers have been extensively investigated in the past decades. However, there is no explicit photogain equation that allows for fitting and designing photoresponses of these devices. In this work, we managed to derive explicit photogain equations for silicon nanowire photoconductors based on experimental observations. The silicon nanowires were fabricated by patterning the device layer of silicon-on-insulator wafers by standard lithography that were doped with boron at a concentration of $\sim 8.6 \times 10^{17}$ cm^{-3}.

$$G = G_{max} \frac{I_{light}^s}{I_{light}} \ln\left(\frac{I_{light}}{I_{light}^s} + 1\right)$$

It was found that the as-fabricated silicon nanowires have a surface depletion region $\sim$32 nm wide. This depletion region protects charge carriers in the channel from surface scatterings, resulting in the independence of charge carrier mobilities on nanowire size. Under light illumination, the depletion region logarithmically narrows down, and the nanowire channel widens accordingly. Photo Hall effect measurements show that the nanowire photoconductance is not contributed by the increase of carrier concentrations but by the widening of the nanowire channel. As a result, a nanowire photoconductor can be modeled as a resistor in connection with floating Schottky junctions near the nanowire surfaces. Based on the photoresponses of a Schottky junction, we derived explicit photogain equations for nanowire photoconductors that are a function of light intensity and device physical parameters. The gain equations fit well with the experimental data, from which we extracted the minority carrier lifetimes as tens of nanoseconds, consistent with the minority carrier lifetime in nanowires reported in literature.

KEYWORDS: photoconductor, explicit gain equation, gain mechanism, silicon nanowire, photo Hall effect
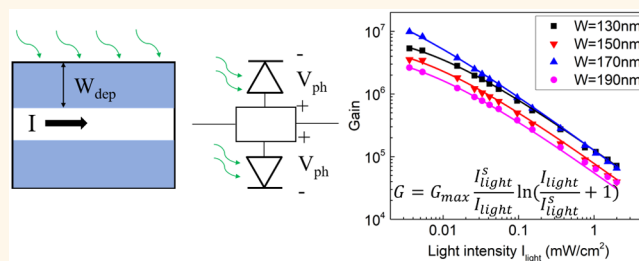
Photoconductors as the simplest photodetectors have been extensively investigated on various semiconducting materials in the past 60 years including thin films,[1,2] nanowires,[3−5] quantum dots,[6,7] and more recently two-dimensional (2D) atomic layers.[8−12] The persistent research interests in photoconductors for decades are mainly driven by the extraordinarily high gain in quantum efficiency (up to 10^{10}) observed in these photoconductors. However, there are still many fundamental issues unsolved in this field after decades of research. First, the classical gain mechanism predicts that high gain is intrinsic to all photoconductors.[2] It often misleads scientists to believe that high-gain and high-speed photoconductors can be made simply by shortening the device length,[13] which however has never been realized. Recently we challenged this gain theory by pointing out that two assumptions in the derivation of the classical gain theory were misplaced.[14] The first assumption is that the classical theory assumes no metal–semiconductor boundary confinement, which leads to the questionable conclusion that high gain can be obtained as long as the minority recombination lifetime is much longer than the transit time. After the metal–semiconductor boundary confinement is considered, it turns

out that a photoconductor intrinsically has no gain or at least no high gain.[14]

However, high gains in photoconductors are often observed in experiments.[3,5,15] The question is where these high gains are coming from.[16−18] This is because the classical theory incorrectly made a second assumption that the number of excess electrons and holes contributing to photoconductivity are equal. Although excess electrons and holes are generated in pairs, excess minority carriers are often trapped by defects or potential wells (depletion regions for instance) in semiconductors.[19,20] The same number of excess majority counterparts is accumulated in the conduction channel, leading to the experimentally observed high photogain.[14]

After the above two assumptions were corrected, we previously derived a gain equation in the same way as the
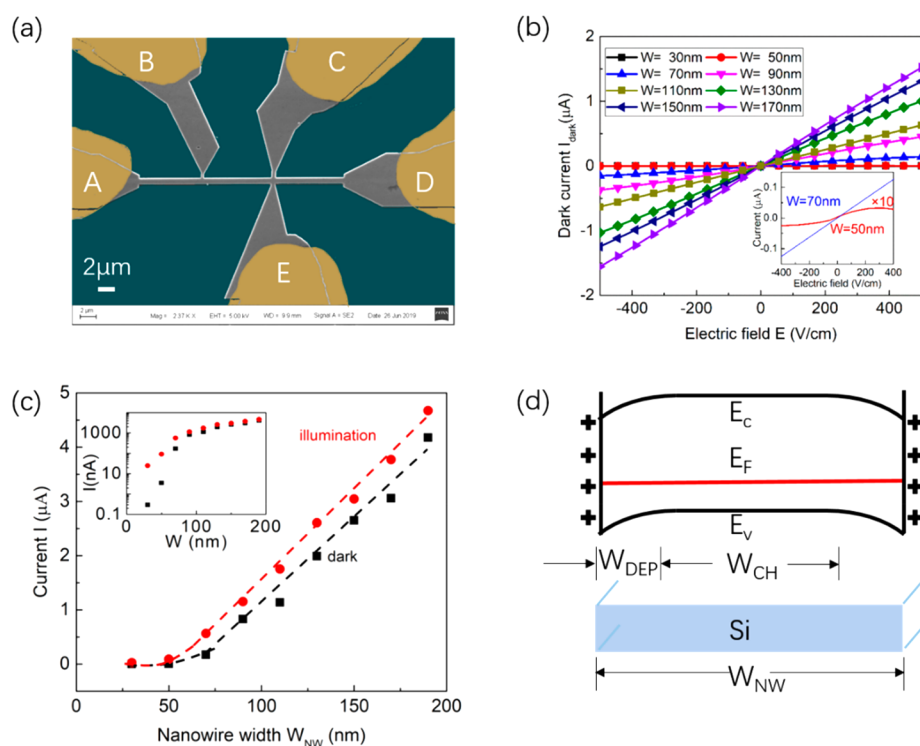
Figure 1. (a) False color SEM image of a silicon nanowire. Si, SiO$_2$, and Au are in gray, dark green, and yellow, respectively. (b) I−V characteristics of typical silicon nanowires with a width ranging from 30 to 190 nm (four-probe measurements). (c) Current at a fixed bias for nanowires with different width in darkness and under light illumination (2 mW/cm^2, λ = 460 nm). Inset: Current in log scale. (d) Energy band diagram in the nanowire cross-section.

classical gain equation was derived.[14] The gain equation can be used to conceptually explain experimental observations of photoconductors. However, similar to the questionable classical gain equation, the gain equation is not an explicit function of light intensity either, but an expression of parameters that are difficult to directly calibrate and design. It is almost impossible to either design the photoconductive gain based on the gain theory or quantitatively check the gain theory against experimental data by fitting.

In this work, we managed to derive explicit photogain equations for single crystalline nanowire photoconductors in which the photogain in quantum efficiency is a function of light illumination intensity and other physical parameters including size, doping concentration, and carrier mobility of underlying devices. These equations may be universal for photoconductors based on isotropic and covalently bonded low-dimensional semiconductors. The derivation is based on the experimental observations that the as-fabricated silicon nanowires have surface depletion regions. Light illumination creates a photovoltage across the depletion regions, which narrows down the depletion regions and therefore increases the channel width. Photo Hall effect measurements indicates that the nanowire photoconductivity is not contributed by the increase of carrier concentrations but the widening of the nanowire channel. As a result, a nanowire photoconductor can be modeled as a resistor in connection with floating Schottky junctions near the nanowire surfaces. The derived photogain equations fit well with the experimental data for all nanowires. From the fitting, we find the effective minority recombination lifetimes in the nanowires are approximately tens of nanoseconds, 2 orders of magnitude lower than that in bulk silicon with a p-type doping concentration of ~10^{18} cm^{-3}. This is

mainly due to the relatively high surface recombination velocity of silicon nanowires and largely consistent with experimental observations reported in literature.[21]

RESULTS AND DISCUSSION

The silicon nanowires along with contact pads were fabricated by patterning the device layer (220 nm thick) of a silicon-on-insulator (SOI) wafer that was heavily doped with boron at a concentration of ~10^{18} cm^{-3} by ion implantation (see Experimental Section for details). These nanowires are 27 μm long with a width ranging from 800 nm down to 30 nm. Figure 1a shows the scanning electron microscopic (SEM) image of a silicon nanowire in contact with five pads for two-probe, four-probe, and Hall effect measurements. The two-probe and four-probe measurements show that the contacts of large pads are ohmic and the contact resistances are negligibly small (see SI Section 1). The four-probe measured dark current *vs* electric field for nanowires with different width is shown in Figure 1b. The current is linear with the applied electric field for the nanowires with a width larger than 60 nm, indicating that the nanowires have a uniform and continuous channel. For those narrower than 60 nm, the current is nonlinearly dependent on the electric field (inset of Figure 1b). The two-probe and four-probe measurements show that this nonlinearity comes from the nanowire channel instead of contacts.

Figure 1c exhibits the current at a fixed bias as a function of nanowire physical width in darkness (black squares) and under light illumination (red dots). In darkness, the current is linear with the nanowire width unless the width is smaller than 65 ± 4 nm, which is extracted from the extension of the linear dependence (Figure 1c). For those nanowires smaller than 65
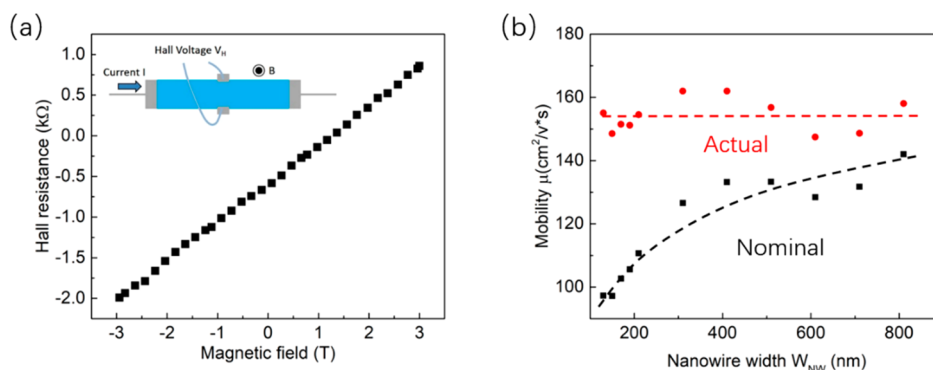
Figure 2. (a) Hall resistance *vs* applied magnetic field of photoconductors. Inset: Schematic of Hall effect measurements on nanowire device. (b) Hole mobility in nanowires with different widths when depletion regions are considered (red dots) or not considered (black squares).
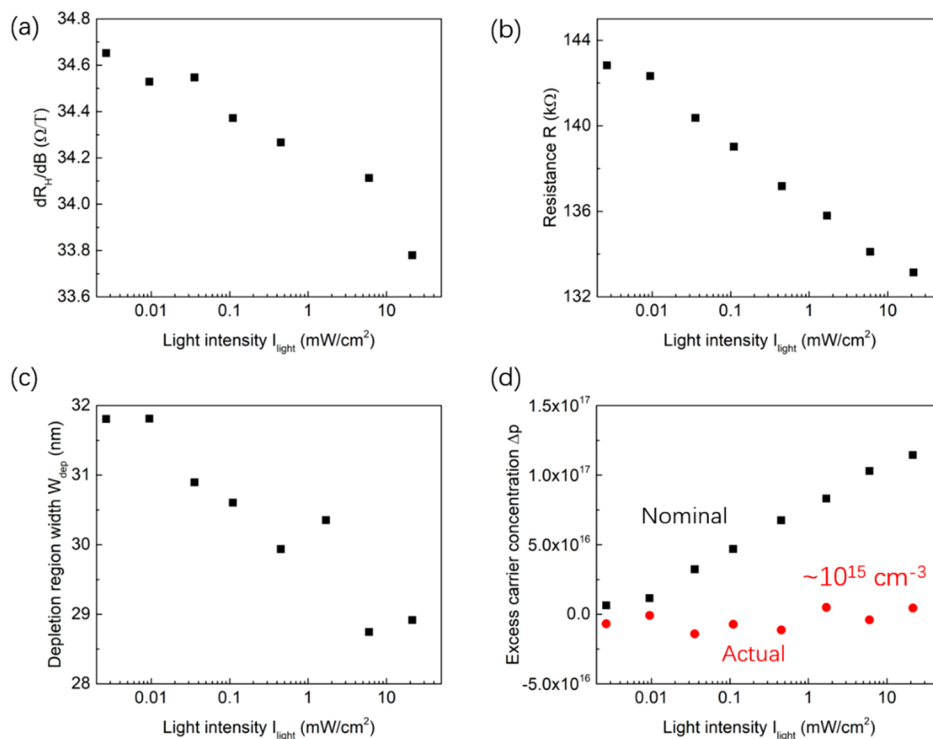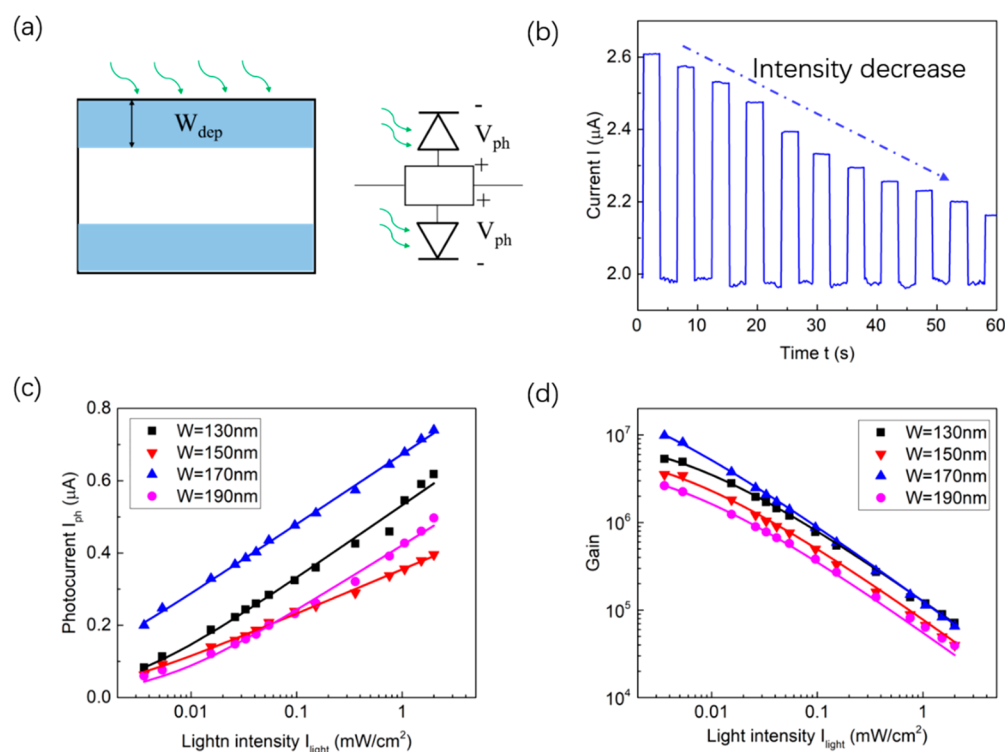

Figure 3. For a 160 nm-wide nanowire device under the illumination of different light intensities (in vacuum at $\lambda = 532$ nm), the following parameters are measured and plotted as a function of light intensity: (a) Derivative of Hall resistance respective to magnetic field, (b) nanowire resistance, (c) depletion region width, and (d) concentration of excess majority carriers when depletion region width is considered (red dots) or not considered (black squares).

± 4 nm, the current follows an exponential dependence on the nanowire width, as shown in the inset of Figure 1c. The only possible explanation is that the nanowire channel is pinched-off by surface depletion regions, as shown in the schematic of Figure 1d (see SI Section 2). The depletion region width is ~32 nm, half of the pinched-off nanowire width. Under light illumination, photogenerated electron−hole pairs will be physically separated by the built-in electric field in the surface depletion region, creating a forward photovoltage across the depletion regions. The forward photovoltage will consequently narrow down the depletion region width and widen the nanowire channel. This is consistent with our experimental observations in which the linear dependence of the nanowire conductance on the wire width is left-shifted under light illumination (red dots in Figure 1c).

The Hall effect measurements were conducted on the nanowires in a physical property measurement system (PPMS-9T, Quantum Design). The charge carriers transporting along the nanowire axial direction are being diverted toward the nanowire sidewalls by the magnetic field, generating a Hall voltage across the nanowire radial direction. The Hall resistance R_H which is linear with the magnetic field can be written as eq 1:

$$R_H = \frac{B}{qH_{ch}p} \qquad (1)$$

where B is the magnetic field, q the unit charge, H_{ch} the thickness of nanowire channel, and p the majority hole concentration in the channel. Considering that SOI wafers have a high-quality Si-SiO$_2$ interface, it is reasonable to assume that the depletion region exists only at the top surface and not

Figure 4. Device model and measured photoresponses of nanowire photoconductors in ambient at $\lambda = 460$ nm. (a) Schematic of equivalent device model for photoconductors. (b) Current of a 130 nm wide nanowire device under chopped illumination of different light intensities. (c) Measured photocurrent of nanowire devices as a function of light intensity. Solid lines are fitting curves following eq 8. (d) Photogain of nanowire photoconductors. Solid lines are fitting curves following eq 9.

at the bottom Si-SiO$_2$ interface. Given that the thickness of the device layer is ~200 nm (some thickness loss after surface cleaning) and the surface depletion region width was previously found as ~32 nm, logically H_{ch} should be equal to ~168 nm. From eq 1 and the linear correlation of Hall resistance and magnetic field, we found the doping concentration in the nanowires as ~8.6 × 10^{17} cm^{-3}. It is known that the nanowire conductance σ is governed by eq 2:

$$\sigma = qp\mu_p H_{ch} W_{ch}/L \qquad (2)$$

where q is the unit charge, μ_p the majority hole mobility, W_{ch} the channel width, H_{ch} the channel height, and L the nanowire length (9 μm long between inner two electrodes in four-probe measurements). Since the conductance, hole concentration, physical dimension of the nanowires, and surface depletion width (from Figure 1c) were measured, we can reliably find the hole mobility μ_p in the nanowire channel from eq 2.

The results are plotted as the red dots in Figure 2b. It shows that the hole mobilities are independent of the nanowire widths, consistent with the fact that there are surface depletion regions near the nanowire surfaces, which keeps the nanowire channel away from the surfaces. The majority hole transport inside the nanowire channel is free from the scattering of surface charges and roughness. However, it was widely reported that the carrier mobilities in semiconductor nanowires are dependent on the nanowire diameters.[22−24] This is because the surface depletion regions were not considered in these works. If we do not consider the surface depletion region either, then the calculated hole mobilities will also decline as the nanowire becomes narrower (black squares in Figure 2b), similar to what was observed by others.[22−24] Given that charge carriers are free of surface effects, the dependence of carrier

mobilities on doping concentration will follow the same correlation as in bulk semiconductors. The hole mobilities around 155 cm^2/(V s) in p-type silicon correspond to a doping concentration of ~1 × 10^{18} cm^{-3},[25] close to the doping concentration ~8.6 × 10^{17} cm^{-3} extracted from Hall effect measurements if the surface depletion regions in the nanowires are taken into consideration.

Under light illumination, the photogenerated electrons and holes both contribute to photoconductivity. Our previous work[4] indicated that the excess majority concentration is orders of magnitude higher than the excess minority concentration in the channel ($\Delta p \gg \Delta n$ in our case). It is because excess minority electrons diffuse into the depletion region, while excess majority holes are accumulated in the nanowire channel due to the built-in electric field of the surface depletion region. In such a case, eqs 1 and 2 will still maintain its present form under light illumination, except $p = p_0 + \Delta p$, $H_{ch} = H_{ch0} + \Delta H_{ch}$ and $W_{ch} = W_{ch0} + \Delta W_{ch}$, where "0" denotes the parameter in darkness. Under light illumination, the product of $H_{ch} \times p$ can be accurately found from eq 1 using the derivative experimental data $\frac{dR_H}{dB}$ in Figure 3a. After the product is plugged into eq 2, the channel width W_{ch} and then the depletion region width (W_{dep}) variation can be reliably found using the measured conductance under light illumination in Figure 3b. Figure 3c exhibits the depletion region width as a logarithm function of light intensity. In fact, from the product of $H_{ch} \times p$, we can find the excess hole concentration Δp as shown in the black squares in Figure 3d on the assumption that H does not change under light illumination. However, light illumination will broaden both H_{ch} and W_{ch} at a similar magnitude due to the narrowing of the surface depletion

region. When this narrowing is considered, the excess hole concentration Δp will be at least 2 orders of magnitude lower (red dots in Figure 3d). This means that the light-induced phenomena in photoconductivity and photo Hall effect are dominantly contributed by the narrowing of the surface depletion region instead of the increase in excess majority carrier concentration, consistent with simulation results in literature.[26]

For this reason, a photoconductor with surface depletion regions can be modeled as a resistor in connection with floating Schottky junctions, as shown in Figure 4a. The depletion region width of the Schottky junction controls the channel width of the resistor. Under light illumination, the photogenerated electron and hole pairs will be separated by the built-in electric field of the Schottky junction, creating a photocurrent I_{ph}^c across the junction (perpendicular to the channel) as eq 3:

$$I_{ph}^c = q \times g \times W_{dep} \times A_{junc} \tag{3}$$

where q is the unit of charge, g the generation rate and A_{junc} the cross-section area of the Schottky junction. The generation rate g is equal to the number of absorbed photons divided by the nanowire volume, that is, $g = \frac{\alpha I_{light} A_{proj}}{\hbar\omega V_{NW}}$, where α is the ratio of the photons absorbed by the nanowire to the total incident ones, A_{proj} is the area of the photoconductors projected in the light incident direction, $\hbar\omega$ is the photon energy, and V_{NW} is the nanowire volume. The absorption ratio α can be found by finite difference time domain (FDTD) simulations for each nanowire (see SI Section S3).

The photocurrent will be balanced by a forward current with a forward voltage (photovoltage) on the floating Schottky junction, as shown in eq 4:

$$I_{ph}^c = A_{junc} J_s \left[\exp\left(\frac{q V_{ph}}{n k_B T} \right) - 1 \right] \tag{4}$$

where J_s is the leakage current density of the Schottky junction, q is the unit charge, k_B is the Boltzmann constant, T is the absolute temperature, and n is the ideality factor. The light intensity can be derived as a function of the photovoltage by plugging eq 3 into eq 4:

$$I_{light} = I_{light}^s \left[\exp\left(\frac{q V_{ph}}{n k_B T} \right) - 1 \right] \tag{5}$$

where $I_{light}^s = \frac{\hbar\omega J_s H}{\alpha W_{dep} q}$ is defined as the critical light intensity, and H is the nanowire physical thickness. The critical light intensity is the light intensity that creates a photocurrent density across the junction equal to the junction leakage current density.

It is known that the built-in potential (V_{bi}) depends on the depletion region width (W_{dep}) as $W_{dep} = \sqrt{\frac{2\varepsilon_s V_{bi}}{q N_A}}$, where ε_s is the silicon dielectric constant, N_A is the acceptor dopant concentration, and q is the unit of charge.[25] Previously we measured the depletion region width as $\sim$ 32 nm and the doping concentration as $\sim 8.6 \times 10^{17}$ cm^{-3}, from which the built-in potential (V_{bi}) can be calculated as 0.70 V. The forward photovoltage will narrow down the Schottky junction depletion region following eq 6. If $\frac{\Delta W_{dep}}{W_{dep}} \leq 20\%$, then the error of eq 6 will be <10%.

$$\Delta V_{bi} = V_{ph} = \frac{2 V_{bi0}}{W_{dep}} \Delta W_{dep} \tag{6}$$

The previous experimental data in Figure 3 show that the nanowire photoconductance is dominantly contributed by the nanowire channel widening. According to eq 2, the nanowire photoconductance will be only a function of the channel cross-section area A_{ch} (= $H_{ch} \times W_{ch}$ in our case) increase. Considering that no surface depletion exists at the bottom surface of the nanowire due to the high-quality Si/SiO$_2$ interface of SOI wafers, the derivative of channel cross-section area A_{ch} respective to W_{dep} is equal to $\left| \frac{dA_{ch}}{dW_{dep}} \right| = 2H_{ch} + W_{ch}$ in our case. For other device structures, this derivative can be found accordingly. The depletion region width variation can be written as

$$\Delta W_{dep} = \frac{I_{ph}}{\mu_p p q E_{ch} \left| \frac{dA_{ch}}{dW_{dep}} \right|} \tag{7}$$

where I_{ph} is the photocurrent, E_{ch} is the electric field intensity in the nanowire, and the other parameters have the same physical meaning as in eq 2. By plugging eq 7 into eq 6 and then into eq 5, we derive the photocurrent as a function of light intensity in eq 8:

$$I_{light} = I_{light}^s \left[\exp\left(\frac{2 q V_{bi0}}{n k_B T} \frac{I_{ph}}{I_{ph}^s} \right) - 1 \right] \tag{8}$$

where $I_{ph}^s = \mu_p p q E_{ch} W_{dep} \left| \frac{dA_{ch}}{dW_{dep}} \right|$ is defined as the critical photocurrent with the parameters given in previous equations. The critical photocurrent is the source-drain photocurrent when the depletion region W_{dep} narrows down to zero by light illumination. Since all the parameters are known, the critical photocurrent can be calculated for different nanowires as shown in the second column of Table 1.

Table 1. Calculated and Extracted Parameters by Fitting Eq 8 to the Data in Figure 4c

NW width (nm)	I_{ph}^s (μA)	n	I_{light}^s (μW/cm^2)	α	J_s (nA/cm^2)	τ_0 (ns)
130	3.07	1.53 ± 0.06	2.28 ± 0.39	0.88	121.2	32.2
150	3.23	0.89 ± 0.02	1.29 ± 0.11	0.85	66.0	59.1
170	3.38	1.34 ± 0.02	0.33 ± 0.02	0.65	13.1	297.6
190	3.54	1.20 ± 0.04	4.79 ± 0.63	0.70	202.3	19.2

Figure 4b exhibits the transient current responses as the light illumination intensity reduces. The resultant photocurrent dependence on light intensity is plotted in Figure 4c for four nanowires. Eq 8 can fit well with the experimental data, from which we can extract the ideality factors n and the critical photocurrent I_{light}^s as summarized in Table 1. The critical light intensity $I_{light}^s = \frac{\hbar\omega J_s H}{\alpha W_{dep} q}$ is correlated with the absorption ratio α, the leakage current density of surface depletion region J_s, and the nanowire surface depletion region width W_{dep}. α can be found for all nanowires by performing FDTD simulations using commercial software Lumerical (fifth column in Table 1). At a given W_{dep} ($\sim$32 nm), we can calculate the leakage
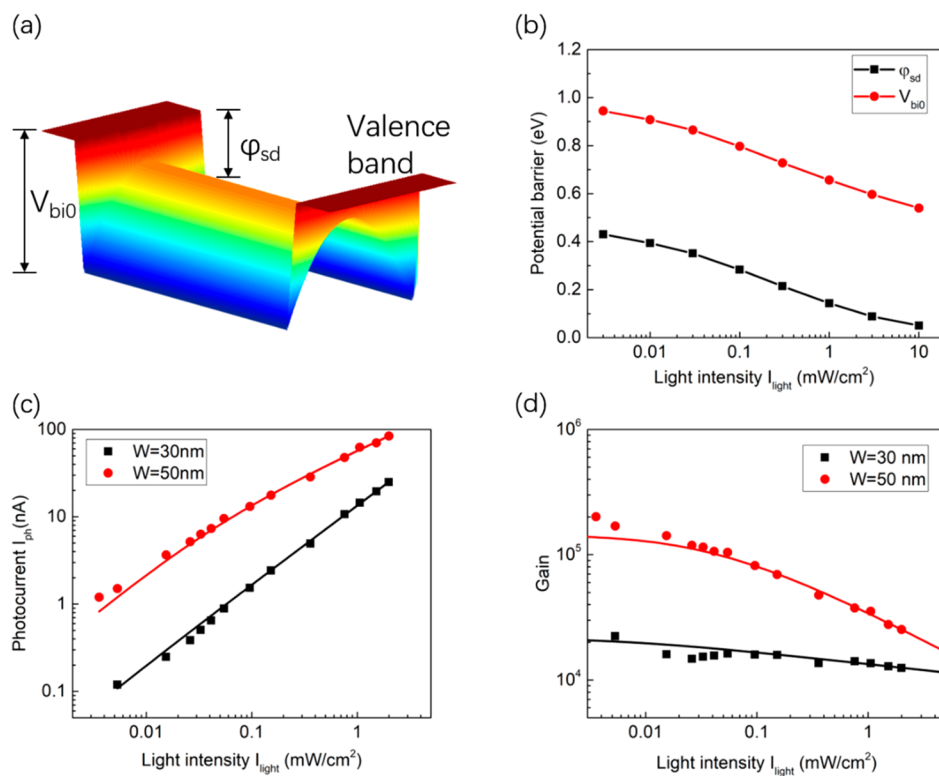
Figure 5. (a) 3D valence band profile of nanowires with a pinched-off channel. (b) Simulated potential barrier V_{bi} and φ_{sd} under illumination (see SI Section 4 for details). (c) Photocurrent current measured at $\lambda = 460$ nm in ambient. Solid lines are fitting curves following eq 13b. (d) Photogain as a function of light illumination intensity. Solid lines are fitting curves following eq 14.

current density J_s from the extracted I_{light}^s for all four nanowires as listed in Table 1. According to semiconductor device physics, the leakage current density J_s in a depletion region can be further written as $J_s = \frac{qn_iW_{dep}}{2\tau_0}$, where q is the unit charge, n_i is the electron concentration in intrinsic silicon, W_{dep} is the depletion region width, and τ_0 is the effective minority carrier recombination lifetime in the doped silicon.[25] The effective minority carrier recombination lifetimes are found to be around tens of nanoseconds (except for the 170 nm wide wire, last column in Table 1), significantly smaller than the bulk minority carrier lifetime for Si at a doping concentration of 10^{18} cm^{-3}. This is caused by strong surface recombination in nanowires as reported in literature.[12,27] The surface recombination velocity can be further estimated on an order of 10^2 cm/s from the nanowire dimensions and the effective minority carrier recombination lifetime.[12]

If the nanowire surface quality is repeatable and the doping concentration is uniform among nanowires, these fundamental parameters n and τ_0 should have similar values from device to device. This is true except that n for the 150 nm wire is clearly smaller and τ_0 for the 170 nm wire is much larger in comparison with the corresponding values of other devices.

For the 150 nm wire, n is smaller due to the clearly smaller slope of photocurrent vs light intensity (red triangles in Figure 4c), but it is unusual for n to be smaller than 1. A possible reason is that the calculated I_{ph}^s is overestimated.

For the 170 nm nanowire, the minority carrier lifetime is much larger since the leakage current is small. When we examine the dark current for this 170 nm nanowire in Figure 1c, we find that the dark current is clearly below the dashed line, indicating that W_{dep} for this nanowire is actually larger

than the average $\sim$32 nm, probably due to a higher concentration of surface states or charges. A careful analysis of Figure 1c shows that the 170 nm nanowire has a depletion region width of $\sim$37 nm, which gives a surface potential of $\sim$0.9 V. The wider surface depletion region is consistent with the fact that the photocurrent for this nanowire is much larger than other nanowires (blue triangles in Figure 4c). The surface potential of $\sim$0.9 V implies that the nanowire surfaces are in strong inversion and a high concentration of electrons is accumulated near nanowire surfaces. The inversion electrons will fill the surface states and reduce the surface recombination velocity (generation in depletion region). As a result, the leakage current density will be smaller.

As a further step, we can find the photogain G from eq 8:

$$G = \frac{I_{ph}/q}{I_{light}A_{proj}/\hbar\omega} = G_{max}\frac{I_{light}^s}{I_{light}}\ln\left(\frac{I_{light}}{I_{light}^s} + 1\right) \tag{9}$$

with

$$G_{max} = \frac{n\hbar\omega k_B T I_{ph}^s}{2q^2 V_{bi0}A_{proj}I_{light}^s} = \frac{2\alpha\varepsilon_s n k_B T\left|\frac{dA_{ch}}{dW_{dep}}\right|}{q^2 n_i W_{dep}A_c}\frac{\tau_0}{\tau_t}$$

where α is the absorption ratio, ε_s is the dielectric constant of the underlying semiconductor, n is the ideality factor, k_B is the Boltzmann constant, T is the absolute temperature, A_{ch} is the channel cross-section area, q is the unit of charge, n_i is the intrinsic electron concentration of underlying semiconductor, W_{dep} is the surface depletion region width, A_c is the device physical cross-section area, τ_0 is the minority carrier recombination lifetime, and τ_t is the majority carrier transit

time across the photoconductor which is equal to $\tau_t = \frac{L}{\mu_p E_{ch}}$, where L is the nanowire length, μ_p is the majority carrier mobility, and E_{ch} is the electric field intensity along the channel. Note that eqs 8 and 9 are valid on the condition that the electric field is not too strong to severely skew the excess carrier distribution due to the metal−semiconductor boundary confinement. Otherwise, the photocurrent will not be linear with applied electric field.[14]

The gain equation fits well with the experimental data shown in Figure 4d. As the light intensity I_{light} gets weaker, the gain approaches to its maximum value G_{max} according to eq 9. Although the maximum photogain is also proportional to the ratio of the minority carrier recombination lifetime to the majority carrier transit time, the high gain does not come from the lifetime ratio but from the channel width modulation by light illumination. This can be seen clearly if we take a closer look at the 130 nm nanowire, for example. The maximum gain for this nanowire can be simplified as $G_{max} = 1.45 \times 10^6 \frac{\tau_0}{\tau_t}$ by plugging the related physical parameters into eq 9. The minority carrier recombination lifetime is ∼32.2 ns, and the carrier transit time is ∼5.3 ns. According to the classical gain theory,[25] the excess carriers will circulate in the circuit ∼6 times (= 32.2/5.3), and the gain will be ∼24 if the mobility difference is taken into account. However, our gain equation predicts the photogain can be as high as ∼10^7 if the light illumination is weak enough, consistent with our experimental measurements. Therefore, it is not surprising that Matsuo et al.[1] observed in 1984 that the gain of GaAs photoconductive detectors predicted by the classical gain theory is at least 3−4 orders of magnitude smaller than the gain measured in the experiments.

For those nanowires narrower than 65 nm, the nanowire channel is pinched off by surface depletion region, creating a potential barrier φ_{sd} between source and drain, like a metal-oxide-semiconductor field effect transistors (MOSFET) operating in subthreshold mode. Similar to the subthreshold current of MOSFET transistors, the current of our pinched-off nanowires also follows a similar correlation with the potential barrier as eq 10:[25]

$$I \sim \exp\left(-\frac{q\varphi_{sd}}{mk_BT}\right)\left[1 - \exp\left(-\frac{qV_{sd}}{k_BT}\right)\right] \quad (10)$$

where k_B is the Boltzmann constant, T is the absolute temperature, q is the unit charge, V_{sd} is the voltage bias between source and drain, φ_{sd} is the minimal potential barrier between source and drain, and m is a factor associated with the energy band bending from nanowire center to surface. Figure 5a exhibits the three-dimensional (3D) energy band diagram for the valence band of the silicon nanowires. The potential barrier φ_{sd} between source and drain is governed by eq 11:

$$\varphi_{sd} = V_{bi0} - \frac{W_{dep}^2 qN_a}{2\varepsilon_s} = V_{bi0} - \frac{W_{NW}^2 qN_a}{8\varepsilon_s} \quad (11)$$

where V_{bi0} is the potential between source/drain and the nanowire surfaces. Since the nanowires are completely pinched off, the depletion region width is equal to half the nanowire physical width, i.e. $W_{dep} = \frac{1}{2}W_{NW}$. The last term in eq 11 is the potential difference from the nanowire center to surfaces. Clearly, the nanowire narrowing will increase the source−drain

potential barrier φ_{sd} and exponentially reduce the dark current, as shown in Figure 1c. Interestingly, the light illumination will not narrow down the center-surface depletion region, since it is limited by the nanowire physical width. As a result, φ_{sd} is locked with V_{bi0}, resulting in the same magnitude of variation by light illumination (not too strong to open the channel) as shown in Figure 5b, i.e. $\Delta\varphi_{sd} \approx \Delta V_{bi0}$ (see SI Section 4 for details). This ΔV_{bi0} is the same ΔV_{bi0} in eq 5 for nanowires with a continuous channel, where the nanowire center-surface potential is equal to the source-surface potential (V_{bi0}). Therefore, we have eq 12 by plugging $\Delta\varphi_{sd} \approx \Delta V_{bi0}$ into eq 5:

$$I_{light} = I_{light}^s\left[\exp\left(\frac{q\Delta\varphi_{sd}}{nk_BT}\right) - 1\right] \quad (12)$$

where n is the ideality factor which should be chosen as ∼1.3 according to Table 1. From eq 10, we can write $\frac{I_{ph} + I_{dark}}{I_{dark}} = \exp\left(\frac{q\Delta\varphi_{sd}}{mk_BT}\right)$. In the end, the photocurrent of photoconductors with a cutoff channel should be correlated with the incident light intensity as eq 13a:

$$I_{light} = I_{light}^s\left[\left(\frac{I_{ph}}{I_{dark}} + 1\right)^{m/n} - 1\right] \quad (13a)$$

, which can be rewritten as

$$I_{ph} = I_{dark}\left[\left(\frac{I_{light}}{I_{light}^s} + 1\right)^{n/m} - 1\right] \quad (13b)$$

The resultant photocurrent as a function of light intensity is plotted in Figure 5c for two pinched-off nanowires. Eq 13b can fit well with the experimental data. From the fitting, we extracted the critical light intensity I_{light}^s and the factor n/m in Table 2. Eq 13a is valid on the condition that the photocurrent

Table 2. Extracted Parameters by Fitting Eq 13b to Figure 5c

NW width (nm)	$I_{light}^s(\mu W/cm^2)$	n/m	α	$J_s(nA/cm^2)$	τ_0 (ns)
30	2.62 ± 0.21	0.90	0.60	94.33	41.1
50	16.37 ± 1.98	0.52	0.49	477.06	8.1

is not too high to turn on the device, which is satisfied in our case. Similar to previous case, the leakage current J_s and minority carrier lifetime can be found from I_{light}^s, the calculated α, and the depletion region width W_{dep} (∼32 nm). The minority carrier lifetime is around tens of nanoseconds, comparable to what was found previously.

Eq 13a is a power function, and it is reasonable to plot it in a log−log scale. For very small nanowires, I_{dark} is extremely small and I_{ph} is often significantly larger than I_{dark}. Eq 13a can be simplified as $I_{light} = I_{light}^s\left(\frac{I_{ph}}{I_{dark}}\right)^{m/n}$. The factor n/m is the slope of photocurrent vs light intensity in a log−log plot, which is often in the range of 0 and 1 as reported for nanowires and other nanomaterials in literature (m/n larger than 1 is also possible). For relatively large nanowires, I_{dark} is not that small, and the photocurrent can be much larger or smaller than I_{dark} depending on light illumination intensity. The 50 nm wide nanowire is in this case. At the high light intensities, the dependence of photocurrent on light intensity is similar to

smaller nanowires with the factor n/m as the slope. At low light intensities, I_{ph} is much smaller than I_{dark}, as a result of which eq 13a can be simplified as $I_{light} \approx I_{light}^s \frac{m}{n} \frac{I_{ph}}{I_{dark}}$. The slope of photocurrent vs light intensity in a log−log plot is approximately equal to 1.

From eq 13b, we can write the photogain as eq 14, which can fit well to the experimental data, as shown in Figure 5d. As the light intensity reduces, the gain approaches a maximum value ($G_{max} = \frac{\hbar\omega}{qA_{proj}} \frac{n}{m} \frac{I_{dark}}{I_{light}^s}$) when the illumination light intensity is much smaller than the critical light intensity ($I_{light} \ll I_{light}^s$).

$$G = \frac{\hbar\omega}{qA_{proj}} \frac{I_{dark}}{I_{light}} \left[\left(\frac{I_{light}}{I_{light}^s} + 1 \right)^{n/m} - 1 \right]$$

$$= G_{max} \left\{ \frac{mI_{light}^s}{nI_{light}} \left[\left(1 + \frac{I_{light}}{I_{light}^s} \right)^{n/m} - 1 \right] \right\} \quad (14)$$

where $G_{max} = \frac{n\hbar\omega I_{dark}}{mqA_{proj}I_{light}^s} = \frac{2n\alpha\tau_0 I_{dark}}{mqn_i V_{NW}}$ where α is the photon absorption ratio, τ_0 is the minority carrier recombination lifetime, I_{dark} is the dark current of the device, q is the unit charge, n_i is the intrinsic electronic concentration of the underlying semiconductor, and V_{NW} is the device physical volume. The maximum photogain G_{max} is proportional to the minority carrier lifetime but irrelative to the carrier transit time. For the 50 nm wide nanowire, the maximum gain G_{max} will be 1.6×10^5, although the minority carrier lifetime is as short as 8.1 ns.

CONCLUSIONS

In this work, we successfully derived two explicit photogain equations for nanowire photoconductors with a continuous and pinched-off channel, respectively. These equations fit well with the experimental data and can be used to quantitatively explain and design photoresponses of nanowire photo-conductors. These explicit gain equations clearly show that the high gain in photoconductors comes from the channel width modulation instead of excess carrier circulation. In terms of universality, these explicit gain equations may be applicable to isotropic and covalently bonded low-dimensional semi-conductors in which interface defects and depletion regions play a dominant role in photoresponses. But the equations are unlikely applicable to 2D materials or other layered and van der Waals bonded structures due to their anisotropic nature.

EXPERIMENTAL SECTION

Si Nanowire Fabrication. The silicon-on-insulator (SOI) wafers were first cleaned with acetone and deionized (DI) water. Boron ions were then implanted into the device layer of the SOI wafer at an implantation energy of 30 keV and a dose of 2.2×10^{13} cm^{-2}. The doping peak is located at 110 nm with a maximum concentration of $\sim 1 \times 10^{18}$ cm^{-3}. After the implantation, rapid thermal annealing (RTA) was employed to activate the boron atoms at 1000 °C for 20 s. Afterward, the silicon wafers were cut into small pieces ($\sim 1 \times 1$ cm^2). Each piece was cleaned with piranha solution (98% H$_2$SO$_4$:30% H$_2$O$_2$, 3:1 (v/v)). A 250 nm-thick layer of poly(methyl methacrylate) (PMMA) resist (XR-1541-006, Dow Corning Electronics, USA) was spin-coated on the p-type SOI samples at 4000 rpm for 60 s. Then, the wafers were baked at 180 °C for 90 s. The PMMA resist was exposed by electron beam lithography (Vistec EPBG5200) and subsequently developed in MIBK and IPA. PMMA is a positive

electron beam resist. After that, aluminum (Al) was evaporated to the exposed region. To form etch mask for the micropads, NR9-1500PY (Futurrex Inc. USA) photoresist was coated on the wafers at 4000 rpm for 40 s. After baked at 140 °C for 60 s, the NR9 resist was exposed to UV light (MDA-400) and developed in the developer after post-baking at 110 °C for 60 s. A 100 nm-thick Al film was evaporated (Thermal Evaporator, Angstrom Engineering), followed by a liftoff process. The Al nanowire and micropad patterns defined by electron beam exposure and photolithography were then transferred to the SOI device layer by reactive ion etching (RIE, Sentech ICP Reactive Ion Etching System), forming an array of silicon nanowires with each connecting to five silicon pads for metal contacts. After photo-lithography, 20 nm-thick cobalt and 180 nm-thick aluminum were evaporated onto the Si pads as electrodes. To form good ohmic contacts, the wafers were then annealed in argon atmosphere for 15 min at 230 °C.

Optoelectronic Measurements. The devices were characterized in a probe station by high-precision digital sourcemeters (Keithley 6487 and 2636). Light from a commercial LED ($\lambda = 460$ nm) forms a uniform light illumination spot (~ 5 mm in diameter) on the samples. The light intensity is controlled by the driving current of the circuit. The light intensity is calibrated by a commercial photodiode (G10899-003 K, Hamamatsu).

ASSOCIATED CONTENT

ⓢ Supporting Information

The Supporting Information is available free of charge at https://pubs.acs.org/doi/10.1021/acsnano.9b09406.

Four-probe and two-probe measurements; simulated potential profile for nanowires with a continuous channel; FDTD simulation; simulated potential profile for nanowires with a cutoff channel (PDF)

AUTHOR INFORMATION

Corresponding Author

Yaping Dan − *State Key Laboratory of Advanced Optical Communication Systems and Networks, University of Michigan − Shanghai Jiao Tong University Joint Institute, Shanghai Jiao Tong University, Shanghai 200240, China; School of Microelectronics, Xi'an Jiao Tong University, Xi'an, Shaanxi 710049, China;* ⓞ orcid.org/0000-0002-2983-7213; Email: yaping.dan@sjtu.edu.cn

Authors

Jiajing He − *State Key Laboratory of Advanced Optical Communication Systems and Networks, University of Michigan − Shanghai Jiao Tong University Joint Institute, Shanghai Jiao Tong University, Shanghai 200240, China*

Kaixiang Chen − *State Key Laboratory of Advanced Optical Communication Systems and Networks, University of Michigan − Shanghai Jiao Tong University Joint Institute, Shanghai Jiao Tong University, Shanghai 200240, China*

Chulin Huang − *School of Microelectronics, Xi'an Jiao Tong University, Xi'an, Shaanxi 710049, China*

Xiaoming Wang − *State Key Laboratory of Advanced Optical Communication Systems and Networks, University of Michigan − Shanghai Jiao Tong University Joint Institute, Shanghai Jiao Tong University, Shanghai 200240, China*

Yongning He − *School of Microelectronics, Xi'an Jiao Tong University, Xi'an, Shaanxi 710049, China*

Complete contact information is available at: https://pubs.acs.org/10.1021/acsnano.9b09406

Author Contributions

§These authors contribute equally.

Author Contributions

Y.D. conceived the idea and derived the theoretical equations. J.H., K.C., and C.H. conducted the experiments. J.H., K.C., and Y.D. analyzed the data. Y.D., J.H., and K.C. wrote the manuscript. C.H. and X.W. performed electronic and optical simulations. Y.H. commented on the manuscript. All authors reviewed the manuscript.

Notes

The authors declare no competing financial interest.

REFERENCES

(1) Matsuo, N.; Ohno, H.; Hasegawa, H. Mechanism of High Gain in GaAs Photoconductive Detectors under Low Excitation. *Jpn. J. Appl. Phys.* **1984**, *23*, L299.

(2) Petritz, R. Theory of Photoconductivity in Semiconductor Films. *Phys. Rev.* **1956**, *104*, 1508−1516.

(3) Kim, C.-J.; Lee, H.-S.; Cho, Y.-J.; Kang, K.; Jo, M.-H. Diameter-Dependent Internal Gain in Ohmic Ge Nanowire Photodetectors. *Nano Lett.* **2010**, *10*, 2043−2048.

(4) Chen, K.; Zhao, X.; Mesli, A.; He, Y.; Dan, Y. Dynamics of Charge Carriers in Silicon Nanowire Photoconductors Revealed by Photo Hall Effect Measurements. *ACS Nano* **2018**, *12*, 3436−3441.

(5) Soci, C.; Zhang, A.; Xiang, B.; Dayeh, S. A.; Aplin, D. P. R.; Park, J.; Bao, X. Y.; Lo, Y. H.; Wang, D. ZnO Nanowire UV Photodetectors with High Internal Gain. *Nano Lett.* **2007**, *7*, 1003−1009.

(6) Konstantatos, G.; Badioli, M.; Gaudreau, L.; Osmond, J.; Bernechea, M.; de Arquer, F. P. G.; et al. Hybrid Graphene-Quantum Dot Phototransistors with Ultrahigh Gain. *Nat. Nanotechnol.* **2012**, *7*, 363.

(7) Konstantatos, G.; Howard, I.; Fischer, A.; Hoogland, S.; Clifford, J.; Klem, E.; et al. Ultrasensitive Solution-Cast Quantum Dot Photodetectors. *Nature* **2006**, *442*, 180.

(8) Mueller, T.; Xia, F.; Avouris, P. Graphene Photodetectors for High-Speed Optical Communications. *Nat. Photonics* **2010**, *4*, 297−301.

(9) Li, H. M.; Lee, D. Y.; Choi, M. S.; Qu, D.; Liu, X.; Ra, C. H.; Yoo, W. J. Metal-Semiconductor Barrier Modulation for High Photoresponse in Transition Metal Dichalcogenide Field Effect Transistors. *Sci. Rep.* **2015**, *4*, 4041.

(10) Lee, J. H.; Gul, H. Z.; Kim, H.; Moon, B. H.; Adhikari, S.; Kim, J. H.; Choi, H.; Lee, Y. H.; Lim, S. C. Photocurrent Switching of Monolayer MoS$_2$ Using a Metal−Insulator Transition. *Nano Lett.* **2017**, *17*, 673−678.

(11) Fang, H.; Hu, W. Photogating in Low Dimensional Photodetectors. *Adv. Sci. (Weinh)* **2017**, *4*, 1700323.

(12) Adinolfi, V.; Kramer, I. J.; Labelle, A. J.; Sutherland, B. R.; Hoogland, S.; Sargent, E. H. Photojunction Field-Effect Transistor Based on a Colloidal Quantum Dot Absorber Channel Layer. *ACS Nano* **2015**, *9*, 356−362.

(13) Jie, J. S.; Zhang, W. J.; Jiang, Y.; Meng, X. M.; Li, Y. Q.; Lee, S. T. Photoconductive Characteristics of Single-Crystal CdS Nanoribbons. *Nano Lett.* **2006**, *6*, 1887.

(14) Dan, Y. P.; Zhao, X. Y.; Chen, K. X.; Mesli, A. A Photoconductor Intrinsically Has No Gain. *ACS Photonics* **2018**, *5*, 4111−4116.

(15) Chen, R.-S.; Yang, T.-H.; Chen, H.-Y.; Chen, L.-C.; Chen, K.-H.; Yang, Y.-J.; Su, C.-H.; Lin, C.-R. High-Gain Photoconductivity in Semiconducting InN Nanowires. *Appl. Phys. Lett.* **2009**, *95*, 162112.

(16) Soci, C.; Zhang, A.; Bao, X. Y.; Kim, H.; Lo, Y.; Wang, D. L. Nanowire Photodetectors. *J. Nanosci. Nanotechnol.* **2010**, *10*, 1430.

(17) Zardas, G. E.; Aidinis, C. J.; Anagnostakis, E. A.; Symeonides, C. I. On a Predictive Scheme of Slow Photoconductive Gain Evolution in Expitaxial Layer/Substrate Optoelectronic Nanodevices. *Open J. Microphys.* **2011**, *1*, 32.

(18) Logeeswaran, V. J.; Oh, J.; Nayak, A. P.; Katzenmeyer, A. M.; Gilchrist, K. H.; Grego, S.; et al. A Perspective on Nanowire Photodetectors: Current Status, Future Challenges, and Opportunities. *IEEE J. Sel. Top. Quantum Electron.* **2011**, *17*, 1002.

(19) Zhao, X. Y.; Tu, P.; He, J. J.; Zhu, H.; Dan, Y. P. Cryogenically Probing the Surface Trap States of Single Nanowires Passivated with Self-Assembled Molecular Monolayers. *Nanoscale* **2018**, *10*, 82−86.

(20) Xu, Q.; Dan, Y. Uncovering the Density of Nanowire Surface Trap States Hidden in the Transient Photoconductance. *Nanoscale* **2016**, *8*, 15934−15938.

(21) Dan, Y.; Seo, K.; Takei, K.; Meza, J. H.; Javey, A.; Crozier, K. B. Dramatic Reduction of Surface Recombination by *In Situ* Surface Passivation of Silicon Nanowires. *Nano Lett.* **2011**, *11*, 2527−2532.

(22) Ford, A. C.; Ho, J. C.; Chueh, Y. L.; Tseng, Y. C.; Fan, Z.; Guo, J.; Bokor, J.; Javey, A. Diameter-Dependent Electron Mobility of InAs Nanowires. *Nano Lett.* **2009**, *9*, 360−365.

(23) Lee, S. H.; Lee, T. I.; Lee, S. J.; Lee, S. M.; Yun, I.; Myoung, J. M. Electrical Characteristics of Metal Catalyst-Assisted Etched Rough Silicon Nanowire Depending on the Diameter Size. *ACS Appl. Mater. Interfaces* **2015**, *7*, 929−934.

(24) Yang, Z. X.; Yip, S.; Li, D.; Han, N.; Dong, G.; Liang, X.; Shu, L.; Hung, T. F.; Mo, X.; Ho, J. C. Approaching the Hole Mobility Limit of GaSb Nanowires. *ACS Nano* **2015**, *9*, 9268−9275.

(25) Neamen, D. A. *Semiconductor Physics and Devices: Basic Principles*, 4th ed.; Mc-Graw-Hill Education: New York, 2011.

(26) Garrido, J. A.; Monroy, E.; Izpura, I.; Muñoz, E. Photoconductive Gain Modelling of GaN Photodetectors. *Semicond. Sci. Technol.* **1998**, *13*, 563−568.

(27) Grumstrup, E. M.; Gabriel, M. M.; Cating, E. M.; Pinion, C. W.; Christesen, J. D.; Kirschbrown, J. R.; Vallorz, E. L.; Cahoon, J. F.; Papanikolas, J. M. Ultrafast Carrier Dynamics in Individual Silicon Nanowires: Characterization of Diameter-Dependent Carrier Lifetime and Surface Recombination with Pump−Probe Microscopy. *J. Phys. Chem. C* **2014**, *118*, 8634−8640.